Current-driven skyrmion motion in granular films

Xin Gong [1], H. Y. Yuan [2,*] and X. R. Wang [1,3,†]

[1] *Physics Department, The Hong Kong University of Science and Technology, Clear Water Bay, Kowloon, Hong Kong*
[2] *Department of Physics, Southern University of Science and Technology, Shenzhen 518055, Guangdong, China*
[3] *HKUST Shenzhen Research Institute, Shenzhen 518057, China*

(Received 6 July 2019; revised manuscript received 27 December 2019; accepted 6 February 2020; published 20 February 2020)

Current-driven skyrmion motion in random granular films is investigated, with interesting findings. For a given current, there exists a critical disorder strength below which its transverse motion could either be boosted below a critical damping or be hindered above the critical damping, resulting in current and disorder dependences of the skyrmion Hall angle. The boosting comes mainly from the random force that is opposite to the driving force (current). The critical damping depends on the current density and disorder strength. However, the longitudinal motion of a skyrmion is always hindered by the disorder. Above the critical disorder strength, skyrmions are pinned. The disorder-induced random force on a skyrmion can be classified as static or kinetic, similar to the friction force in the Newtonian mechanics. In the pinning phase, the static (pinning) random force is against the tendency direction of skyrmion motion that is transverse to the current density for spin-transfer-torque-driven motion. The kinetic random force is opposite to the skyrmion velocity when skyrmions are in motion. Furthermore, we provide strong evidences that the Thiele equation can perfectly describe skyrmion dynamics in granular films. These findings provide insight into skyrmion motion and should be important for skyrmiontronics.

DOI: 10.1103/PhysRevB.101.064421

I. INTRODUCTION

Magnetic skyrmions have attracted much attention in recent years because of their potential applications in information storage and processing, in addition to their academic interest [1–46]. This potential can be realized only when a good understanding of the disorder effect on skyrmion motion is obtained because defects and inhomogeneity exist inevitably in all materials. There are a few studies [36–48] of skyrmions in disordered systems. Many phenomena were observed with limited understanding. For example, in the presence of isolated impurities, micromagnetic simulations suggest that skyrmions sometimes avoid impurities [37] and sometimes are trapped by disorders [40]. There is no well-accepted understanding of these seemingly conflicting results. The ability of a skyrmion to avoid trapping with trajectory detoured away from isolated defects was attributed to its topological properties [37]. This interesting ability leads to the theoretical prediction [37] that disorders have few effects on skyrmion driving current density. Just like their counterparts in a uniform film, skyrmions in a disordered film should move under a current density as low as 10^5–10^6 A/m^2, five orders of magnitude smaller than that for a domain wall [37]. However, experimentally reported driven current is above 10^{10}–10^{11}A/m^2 [32,34,36], not too far from the typical magnetic domain wall driving current and far above the community's expectation. Skyrmions can also perform a random-walk-like motion in a disordered system [49]. All these issues and more need a detailed analysis and better understanding.

In this paper, we study the influences of disorders on skyrmion motion. Our numerical and analytical results show that disorders could boost skyrmion transverse motion under certain conditions, while they always hinder skyrmion longitudinal motion. Thus, disorders boost skyrmion Hall angle. The physics behind the respective boosting and hindering of the transverse and longitudinal motions is mainly from the random forces along the driving force direction: When the random force is opposite the driving force, skyrmion transverse speed increases, while the longitudinal speed decreases. In the opposite case when the random force is along the driving force, the transverse speed decreases, and the longitudinal speed increases. As a result, the duration time of a skyrmion with a larger transverse speed and a smaller longitudinal speed is longer than that in the opposite situation. This explains the boosting of the time-averaged transverse skyrmion speed and the hindering of the average longitudinal speed in disorders. In comparison, the random force transverse to the current direction decreases or increases both transverse and longitudinal skyrmion speeds at the same time. To the first-order effect, the random force has little effect on average skyrmion velocity along the transverse direction.

This paper is organized as follows. In Sec. II, we first describe the model and approach adopted in this study. Section III presents our main findings, including three phases, the origin of the boosting of skyrmion transverse motion, static and kinetic random forces, and how accurate the Thiele equation is in describing skyrmion motion in granular films. Interestingly, the average random force on a moving skyrmion is opposite the skyrmion velocity. In the discussion, we point

*huaiyangyuan@gmail.com
†phxwan@ust.hk

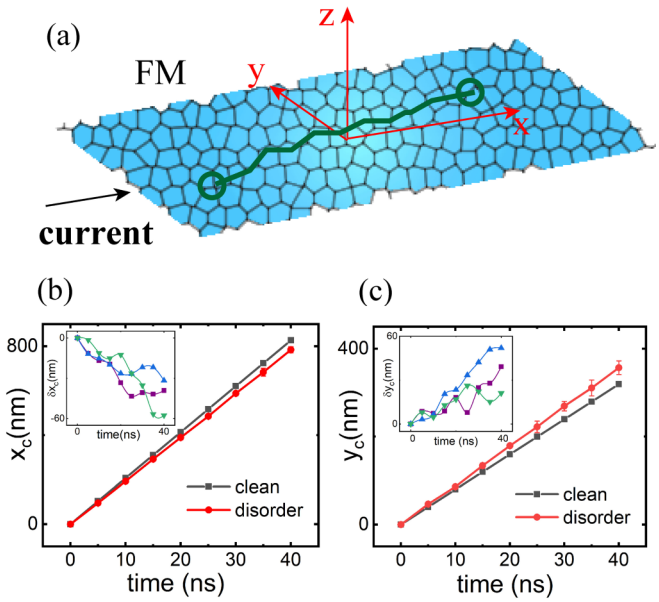

FIG. 1. (a) Schematic illustration of a skyrmion in a granular chiral magnetic film with randomly distributed anisotropy. (b) and (c) Time evolution of ten ensemble-averaged skyrmion positions $\vec{R} = (x_c,\ y_c)$ under an electric current for a granular film of $\Delta K = 3\%K_0$ (red dots). For a comparison, the black squares are for a homogeneous film. The inset shows the position difference between the homogeneous and three typical granular films. The three curves are for three different realizations. The model parameters are $\alpha = 0.3,\ \beta = 0,\ J = 6 \times 10^{11}\ \mathrm{A/m^2}$.

out the fundamental differences between disorder-induced domain wall motion boosting and skyrmion motion boosting and show that the physics presented here does not change when the fieldlike torque is present as long as its value is smaller than the damping coefficient. We will also discuss the spin-orbit-torque-driven skyrmion motion. The conclusion is given in Sec. IV.

II. MODEL AND METHODOLOGY

We consider a perpendicularly magnetized random granular film that is constructed by a Voronoi tessellation, as shown in Fig. 1(a). Magnetic anisotropy K in each grain is randomly distributed around $K_0 = 8.0 \times 10^5\ \mathrm{J/m^3}$ either with a Gaussian distribution of deviation ΔK or uniformly in a window of $(K_0 - \Delta K, K_0 + \Delta K)$. The granular film with the Gaussian distribution is assumed below if not otherwise specified.

The material parameters are chosen in such a way that supports a stable isolated skyrmion [24]. Initially, a skyrmion is located in the center (also the origin of the xyz coordinate). Spin dynamics is governed by the Landau-Lifshitz-Gilbert (LLG) equation,

$$\frac{\partial \vec{m}}{\partial t} = -\gamma \vec{m} \times \vec{H}_{\mathrm{eff}} + \alpha \vec{m} \times \frac{\partial \vec{m}}{\partial t} + \vec{\tau}, \tag{1}$$

where $\vec{m}$, γ, and α are, respectively, the unit vector of the magnetization, gyromagnetic ratio, and the Gilbert damping. $\vec{H}_{\mathrm{eff}} = 2A\nabla^2\vec{m} + 2Km_z\hat{z} + \vec{H}_d + \vec{H}_{\mathrm{DM}}$ is the effective field including the exchange field characterized by the exchange stiffness A, crystalline anisotropy field along the z direction, dipolar field $\vec{H}_d$, and the Dzyaloshinskii-Moriya interaction (DMI) field $\vec{H}_{\mathrm{DM}}$ characterized by the DMI coefficient D. In this study, we consider the interfacial DMI with a DMI energy density of $D[(\hat{z}\cdot\vec{m})\nabla\cdot\vec{m} - (m\cdot\nabla)(\hat{z}\cdot\vec{m})]$. $\vec{\tau} = -(\vec{u}\cdot\nabla)\vec{m} + \beta\vec{m}\times(\vec{u}\cdot\nabla)\vec{m}$ is the spin transfer torque consisting of a dampinglike torque and a fieldlike torque [50,51], where β is a dimensionless coefficient measuring the strength of the fieldlike torque and $\vec{u} = \vec{J}P\mu_B/(eM_s)$ is a quantity of the dimension of speed measuring the amount of equivalent magnetic moments supplied from spin-polarized current to the magnet per unit time. Here J, P, μ_B, e, and M_s are, respectively, current density, current polarization, the Bohr magneton, the electron charge, and the saturation magnetization. To study the skyrmion dynamics, we use the MUMAX3 package [52] to numerically solve the LLG equation on a granular film with a size of $1024 \times 512 \times 1\ \mathrm{nm^3}$. The mesh size is $1 \times 1 \times 1\ \mathrm{nm^3}$ so that no change in simulation results is observed when a smaller mesh size is used (see the Appendix for the results with a smaller mesh size). The average grain size is 5 nm, and the model parameters are $A = 15 \times 10^{-12}\ \mathrm{J/m}$, $D = 0.003\ \mathrm{J/m^2}$, $M_s = 5.8 \times 10^5\ \mathrm{A/m}$ in this study. The size of our skyrmions is about 7 nm, comparable to the grain size. This is expected to be the most interesting case. For a grain size much smaller than the skyrmion size, the disorder effect will be averaged out and become less pronounced. In the opposite limit of grain size much larger than the skyrmion size, a skyrmion moves most of the time in a homogeneous region, so that the disorder effect is again less pronounced.

To understand the skyrmion dynamics, we derive the Thiele equation in disorders by recasting Eq. (1) as $\partial_i\vec{m}\cdot(\vec{m}\times$ Eq. (1)). Under the rigid-body assumption and after some algebra, we obtain following equation for skyrmion velocity $\vec{v}$:

$$\vec{G}\times(\vec{v}-\vec{u}) + \overleftrightarrow{D}\cdot(\alpha\vec{v} - \beta\vec{u}) + \frac{\gamma}{M_s d}\nabla E = 0, \tag{2}$$

where d is the film thickness, $\vec{G} = G\hat{z} = 4\pi Q\hat{z}$ is the skyrmion gyrovector proportional to the skyrmion number Q [24], and the tensor $D_{ij} = \int \partial_i\vec{m}\cdot\partial_j\vec{m}dxdy$ is the dissipation dyadic. For symmetric skyrmion structures, $D_{ij} = D\delta_{ij} = \frac{1}{2}(R/w + w/R)\delta_{ij}$, where R and w are, respectively, skyrmion size and skyrmion wall width [24]. $E(\vec{R}) = \int\int\{A(\nabla\vec{m})^2 + D[(\hat{z}\cdot\vec{m})\nabla\cdot\vec{m} - (m\cdot\nabla)(\hat{z}\cdot\vec{m})] - K(\vec{x},\vec{y})m_z^2\}dxdydz$ is the total energy of a skyrmion centered at position $\vec{R}$. In a homogeneous film, the total energy of the skyrmion does not depend on the skyrmion position ($\nabla E = 0$) due to the translational symmetry of the system. Equation (2) is the original equation derived by Thiele [53]. In a granular film, the translational symmetry is broken so that $\nabla E \neq 0$. $\vec{F} \equiv -\frac{\gamma}{M_s d}\nabla E$ is a random force in all directions when a skyrmion is in motion. Let us first consider $\beta = 0$ and $\vec{F} = (F_x, F_y)$; Eq. (2) becomes

$$Gv_x + \alpha D v_y = Gu + F_y, \tag{3a}$$

$$Gv_y - \alpha D v_x = -F_x. \tag{3b}$$

Without losing generality, we set $Q = 1$ and assume $u > 0$. The solution of the above equations is $v_x = [G^2u + GF_y + \alpha DF_x]/[G^2 + (\alpha D)^2]$, $v_y = [\alpha DGu + \alpha DF_y - GF_x]/[G^2 + (\alpha D)^2]$. In a homogeneous film, we have

$F_x = F_y = 0$ and $v_y > 0$ and $0 < v_x < u$ since $\alpha D > 0$. Furthermore, the skyrmion Hall angle does not depend on u (current). For a negative F_x and $F_y = 0$, v_y increases while v_x decreases, so that skyrmion Hall angle increases and depends on both disorders and u. In the opposite case of a positive F_x and $F_y = 0$, v_y decreases while v_x increases, so that the skyrmion Hall angle becomes smaller. In contrast, v_x and v_y vary with F_y differently when $F_x = 0$: v_x and v_y increase or decrease simultaneously for $F_y > 0$ and $F_y < 0$, respectively. These dependences of v_x and v_y are important for us to understand the boosting of the skyrmion transverse discussed below.

III. RESULT

A. Three phases

Figures 1(b) and 1(c) plot skyrmion positions $\vec{R} = (x_c, y_c)$ as a function of time for a homogeneous film (black squares) and for a granular film (red dots) of $\Delta K = 3\%K_0$ for $\alpha = 0.3$, $\beta = 0$, $J = 6 \times 10^{11}$ A/m^2. x_c and y_c for the granular film are the ensemble average over ten independent realizations. The inset shows the position differences of three typical granular films and the homogeneous film. The trajectory of skyrmion motion in the homogeneous film is a perfectly straight line with constant velocity, while it wiggles around a straight line in each realization of the random granular film, as shown in the insets. The ensemble average of $x_c(t)$ and $y_c(t)$ is perfectly linear, so that the average skyrmion velocity $\vec{v}$ is a good description of skyrmion motion. The average longitudinal and transverse skyrmion velocities are $v_x = 19.7$ m/s and $v_y = 8.9$ m/s for random granular films, and $v_x = 20.7$ m/s and $v_y = 8.0$ m/s for the homogeneous film, which agree perfectly with solution of Eq. (2) with $\nabla E = 0$ (black lines). Interestingly, the transverse motion is boosted by the disorder, while the longitudinal motion is hindered.

One can compute the average skyrmion velocity and its statistical errors from different realizations and for different disorder strengths and Gilbert damping. Figure 2 shows how average v_y and its error bar vary with the disorder strength $\Delta K/K_0$ (as a percentage) for current density $J = 6 \times 10^{11}$ A/m^2 and $\alpha = 0.6$ [Fig. 2(a)] and $\alpha = 0.3$ [Fig. 2(b)]. Points of zero velocity correspond to the skyrmion pinning, similar to the magnetic domain wall pinning by disorders or notches [54–56]. The critical disorder strength, above which all skyrmions are pinned, depends on the current density J (proportional to u). In the cyan region, the average transverse velocity in the granular film is larger than that in the homogeneous film, and the system is in the boosting phase. As disorder strength $\Delta K/K_0$ increases, the error bars increase, and the average transverse velocities in disorder systems increase parabolically for $\alpha = 0.3$. For a larger disorder strength $\Delta K/K_0 > 4\%$, the skyrmions are in the pinning phase (red region). The inset shows a linear J dependence of the critical disorder $\Delta K/K_0$, like the effect of the friction force in Newtonian mechanics in which one needs a larger driven force to maintain the motion of a body on a rougher surface. The physics does not depend on whether the distribution function of random K is Gaussian or uniform in a window. As shown in Fig. 2(c) for K uniformly distributed in a window of $[K_0 - \Delta K, K_0 + \Delta K]$, one can clearly see both boosting and pinning. The only difference is at the qualitative level.

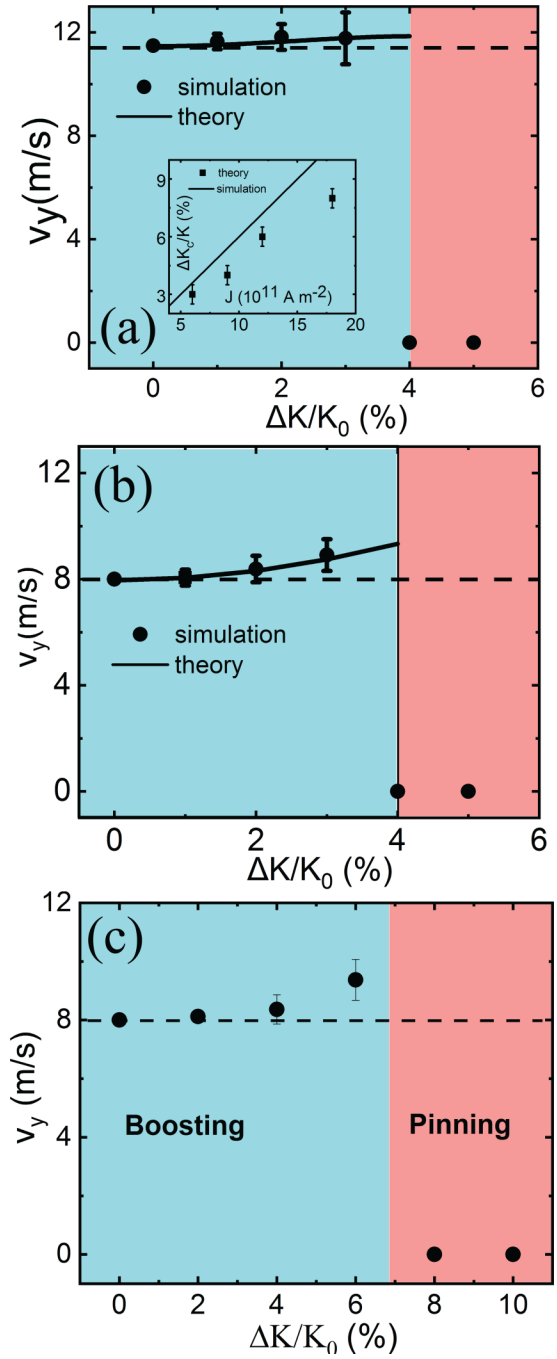

FIG. 2. Disorder strength dependence of skyrmion transverse velocity for $J = 6 \times 10^{11}$ A/m^2. The Gaussian distribution of magnetic anisotropy with (a) $\alpha = 0.6$ and (b) $\alpha = 0.3$. (c) The same plot for the uniform distribution of magnetic anisotropy with $\alpha = 0.3$. The horizontal dashed line is v_y of the homogeneous film, while dots are simulation results, and the solid line is the solution of Eqs. (2) and (4) for $\beta = 0$ with a fitting parameter b defined in random force f. Cyan and red denote the boosting phase and pinning phase, respectively. The inset shows the critical disorder strength as a function of the current density for $\alpha = 0.3$, $\beta = 0$; the black squares are numerical results.

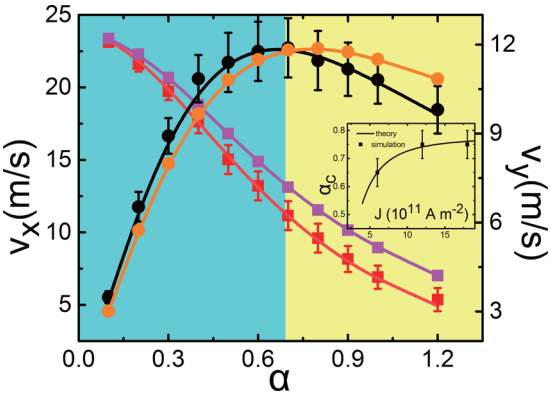

FIG. 3. The α dependence of longitudinal (squares) and transverse (dots) velocities for $J = 6 \times 10^{11}$ A/m^2 and $\Delta K = 3\%K_0$. Purple and orange denote the velocities in the homogeneous film, while black and red are for the granular film. The lines are the solutions of Eqs. (2) and (4) with b in f (for the granular film) as a fitting parameter. Cyan and yellow denote the boosting phase and hindering phase, respectively. The inset shows the current density dependence of critical damping. Other parameters are $\beta = 0$ and those specified in the model.

Figure 3 shows how v_x (squares) and v_y (dots) change with the Gilbert damping coefficient α for $J = 6 \times 10^{11}$ A/m^2, $\beta = 0$, and $\Delta K = 3\%K_0$. Different from v_x that monotonically decreases with α (red), v_y (black) increases first and then decreases with α, as shown in Fig. 3. To see the boosting and hindering effect, we have also plotted v_x and v_y for the homogeneous film (purple and orange, respectively) for the same model parameters. Obviously, skyrmion transverse motion is boosted or hindered by the disorder for $\alpha < 0.7$ or $\alpha > 0.7$. Interestingly, the critical damping that separates boosting from hindering coincides with the peak position of v_y. The longitudinal motion is, however, always hindered by the disorder in our simulations. The value of the critical damping coefficient depends on the current density, as shown in the inset.

In summary, three phases are identified: The pinning phase above the critical disorder strength, boosting of skyrmion transverse motion below the critical disorder strength and below a critical damping coefficient, and hindering of skyrmion transverse motion below the critical disorder strength and above the critical damping. Both the critical disorder strength and critical damping coefficient depend on the applied current density and other model parameters. Numerically, critical damping α_c at disorder strength $\Delta K_c/K_0 = 3\%$ seems to coincide with the peak position of v_y.

B. Origins of boosting

To understand the origins of the boosting of skyrmion transverse motion, we consider how a skyrmion crosses a y-aligned boundary [Fig. 4(a)] and an x-aligned boundary [Fig. 4(b)] that separates two otherwise homogeneous magnetic films. For a y-aligned boundary, the boundary force on a rightward-moving skyrmion is along the positive x direction, $F_x > 0$, when the magnetic anisotropy of the film on the left is larger than K on the right (all other model parameters are

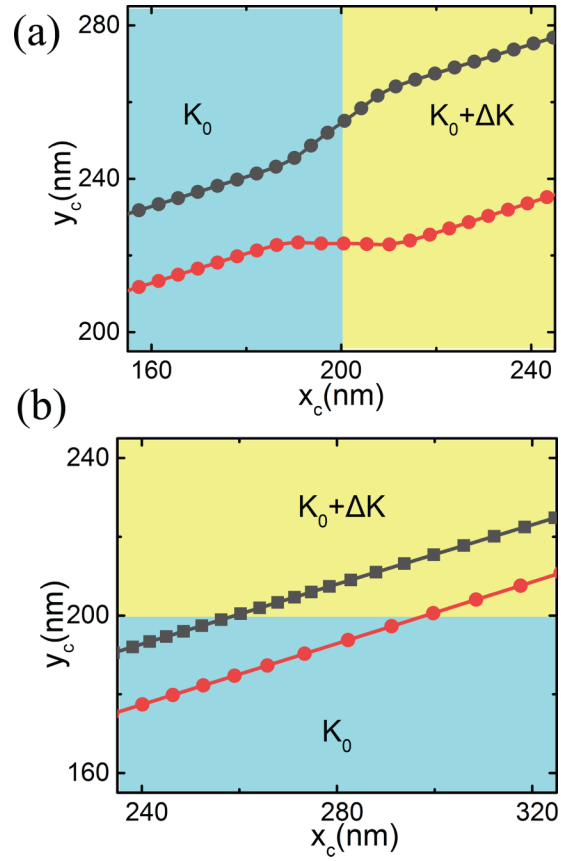

FIG. 4. Model parameters are $J = 6 \times 10^{11}$ A/m^2, $\alpha = 0.3$, $\beta = 0$, and $K_0 = 8.0 \times 10^5$ J/m^3, as well as those specified in the model. (a) A y-aligned boundary. The anisotropy is K_0 on the left of the boundary and $K_0 + \Delta K$ on the right of the boundary. The lines indicate the skyrmion trajectories when it cross the boundary from the left. The black line is for $\Delta K = 3\%K_0$ ($F_x < 0$), and the red line is for $\Delta K = -3\%K_0$($F_x > 0$). (b) A x-aligned boundary. The anisotropy is $K_0 + \Delta K$ above the boundary and K_0 below the boundary. The lines indicate the skyrmion trajectories when it cross the boundary from the bottom. The black line is for $\Delta K = 3\%K_0$ ($F_y < 0$), and the red line is for $\Delta K = -3\%K_0$ ($F_y > 0$).

the same as specified earlier). Figure 5(a) shows clearly that the average transverse velocity (downward triangles) becomes smaller, while the longitudinal velocity (dots) is larger near the boundary. The skyrmion trajectory (red dots and line) is deflected towards the x direction near the boundary, as indicated by the red line in Fig. 4(a).

If K on the left is smaller than K on the right, the boundary force is negative, $F_x < 0$, and v_y (upward triangles) is larger near the boundary, while v_x (squares) becomes smaller near the boundary shown in Fig. 5(a). Thus, the skyrmion trajectory is deflected towards the y direction near the boundary, as indicated by the black dots and line in Fig. 4(a). This feature was also observed by others [57] and was termed the gliding motion of skyrmions. However, its true origin was not sufficiently revealed. It should be pointed out that all the lines in Fig. 5 are the numerical solutions of Eq. (2) in which E and $\overleftrightarrow{D}$ are numerically computed from the spin structures in simulations that vary with time. The perfect

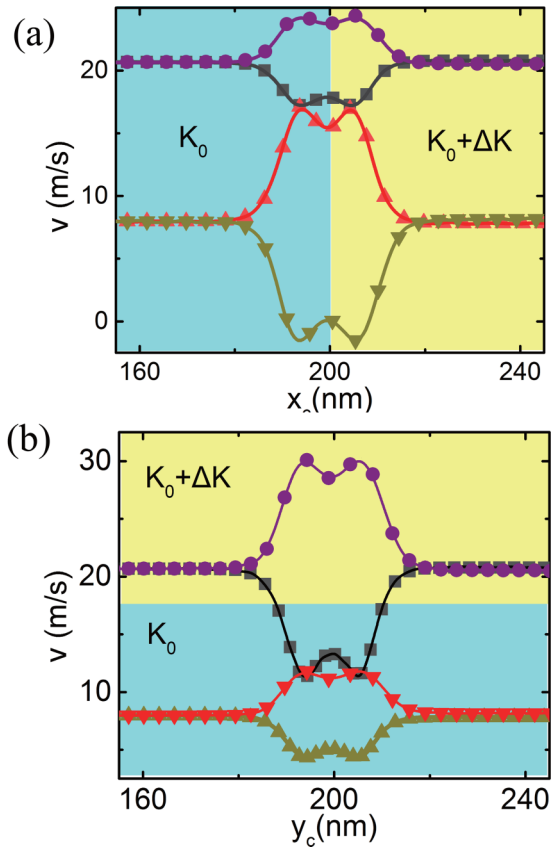

FIG. 5. Model parameters are $J = 6 \times 10^{11}$ A/m^2, $\alpha = 0.3$, $\beta = 0$, and $K_0 = 8.0 \times 10^5$ J/m^3, as well as those specified in the model. (a) v_x and v_y at different positions for a y-aligned boundary. Squares and upward triangles are for simulation results of v_y and v_x, respectively, for $\Delta K = 3\%K_0$, while dots and downward triangles are for v_y and v_x for $\Delta K = 3 - \%K_0$. (b) v_x and v_y at different positions for an x-aligned boundary. The squares and the upward triangles are for simulation results of v_x and v_y, respectively, for $\Delta K = 3\%K_0$, while dots and downward triangles are for $\Delta K = -3\%K_0$. All lines are numerical solutions of Eq. (2) in which instantaneous E and $\overleftrightarrow{D}$ obtained from the skyrmion structure are used.

agreement between micromagnetic simulations and numerical solutions of Eq. (2) demonstrates the excellent approximation of the Thiele equation, although the rigid-body assumption is obviously invalid for a skyrmion crossing a boundary. For randomly distributed disorders, the sizes of regions with $F_x > 0$ and $F_x < 0$ should be the same, so that a skyrmion spends more time staying in $F_x < 0$ regions than in $F_x > 0$ ones. As a result, the time-averaged skyrmion transverse velocity is boosted, while the longitudinal velocity is hindered.

In contrast, when a skyrmion crosses an x-aligned boundary [Fig. 4(b)], both v_x (dots and squares) and v_y (downward triangles and upward triangles) increase near the boundary for $F_y > 0$ and decrease near the boundary for $F_y < 0$, as shown in Fig. 5(b). Again, the lines are the numerical solutions of Eq. (2). Different from the effect of F_x, random force in the transverse direction has little effect on the skyrmion Hall angle because it increases (decreases) longitudinal and transverse velocities simultaneously, so that skyrmion trajectories show negligible deflection when skyrmions cross the boundary, as

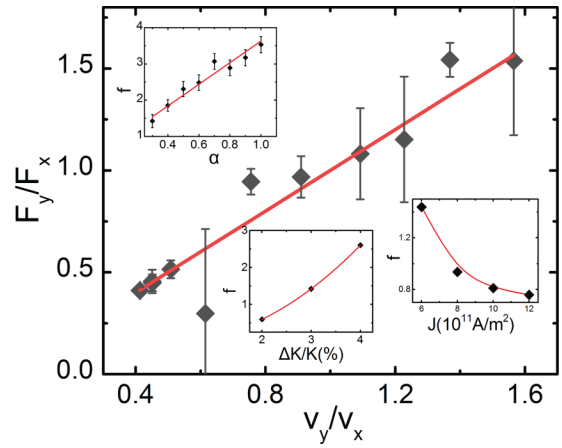

FIG. 6. F_y/F_x vs v_y/v_x for various J, ΔK, and α. All other model parameters are specified in the section of the model. Solid diamonds are the numerical data, and the black line is for $y = x$. All (F_y/F_x, v_y/v_x) fall around the line. The insets show the f dependence on J, ΔK, and α.

shown by the red and black lines in Fig. 4(b). From Fig. 5(b), a velocity difference of about 0.1 m/s in the left and right domains far away from the boundary is observed, which is much smaller than the boundary effect. Thus, the influence of the boundary force and small variation of $\overleftrightarrow{D}$ in different domains will be neglected in the following analysis. Following the same analysis as in the case of F_x, we found weak hindering of both v_x and v_y. In summary, both y-aligned and x-aligned boundary effects lead to the hindering of longitudinal motion. However, the y-aligned boundary effect is the main cause of boosting of transverse motion.

C. Random force at pinning and in motion

In order to have a better understanding of the three phases, we would like to consider the random force defined in Eqs. (2) and (3). For simplicity, we consider only the case of $\beta = 0$. When a skyrmion is at rest, then the random force should balance the driven force from current $\vec{u}$ that tends to move the skyrmion perpendicularly to the driven current, i.e., $\vec{F} = \vec{G} \times \vec{u}$. Thus, the static random (pinning) force must be transverse to the current direction. To study the random force on a skyrmion when it moves in a random potential landscape, we would like to numerically verify our conjecture that, like the friction force of an object moving on a surface that is always opposite its velocity in Newtonian mechanics, the average random force is also opposite the skyrmion motion. Since the Thiele equation is an excellent description of skyrmion dynamics in domains and crossing domain boundaries, we can substitute the instantaneous skyrmion velocity obtained from the micromagnetic simulations into Eq. (3) to obtain the numerical random force for a given system at each moment. Obviously, this is a stochastic quantity that varies from time to time. In terms of skyrmion motion, the meaningful quantity is the time-averaged random force. Below, all F_x and F_y are the time-averaged values for each given system. One can obtain different pairs of (F_y/F_x, v_y/v_x) by using different J, α, and ΔK, and they should fall on line $y = x$ if $\vec{F} \parallel -\vec{v}$. Figure 6

plots points $(F_y/F_x,\ v_y/v_x)$ in the $F_y/F_x - (v_y/v_x)$ plane. It is clear that all points $(F_y/F_x,\ v_y/v_x)$ lie, indeed, around line $y = x$, strong numerical evidence that the direction of $\vec{F}$ is opposite skyrmion velocity,

$$\vec{F} = -f\hat{v}, \tag{4}$$

where $\hat{v}$ is the unit direction of skyrmion velocity.

f depends on the driven current, disorder strength, and the skyrmion structure. From Eq. (3), the average velocity $v_x = \frac{G^2u-(\alpha DF_x)^2/G^2u}{G^2+(\alpha D)^2}$, and $v_y = \frac{\alpha DGu+\alpha DF_x^2/Gu}{G^2+(\alpha D)^2}$. Assuming the regions of $F_x < 0$ and $F_x > 0$ are the same, the time-averaged random force should be $F = F_x(1/v_{x1} - 1/v_{x2})/(1/v_{x1} + 1/v_{x2}) = -F_x(v_{x1} - v_{x2})/(v_{x1} + v_{x2}) \simeq -(\alpha DF_x^2)/G^2u$, where v_{x2} (v_{x1}) is the velocity under random force $-F_x$ (F_x). This suggests that f takes the form of $f = b\alpha D\Delta K^2/J = b\alpha D\delta/u$, where $\delta \equiv \Delta K^2 P\mu_B/(eM_s)$ measures disorder strength and has a dimensionality of velocity. b is a dimensionless and position-independent numerical factor of the order of 1. To test this reasoning, we numerically plot f against α, ΔK, and J in the insets of Fig. 6. As shown in the insets, f is proportional to α and ΔK^2 but inversely proportional to J, as conjectured.

We can test how good this f is by substituting Eq. (4) into Eq. (3) and solving for $\vec{v}$ as a function of $\Delta K/K$ and αD by treating b as the only fitting parameter. For the small pinning strength $(\Delta K/K_0 \leqslant 3\%)$, we carried out the calculation for the model parameters used for simulations in Figs. 2 and 3, and the lines are the theoretical results. Almost perfect agreement between the simulation results and numerical solution of Eq. (3) demonstrates not only the high accuracy of the Thiele equation but also the excellent approximation of f.

D. Phase diagram

By substituting $\vec{F}$ in Eq. (4) into the generalized Thiele equation (2), we can solve the equation for skyrmion velocity,

$$v_x = \frac{G^2}{G^2 + (\alpha D + f/v)^2}u, \tag{5a}$$

$$v_y = \frac{G(\alpha D + f/v)}{G^2 + (\alpha D + f/v)^2}u, \tag{5b}$$

$$v = \frac{\sqrt{(u^2 - f^2)[G^2 + (\alpha D)^2] + \alpha^2D^2f^2} - \alpha Df}{G^2 + (\alpha D)^2}, \tag{5c}$$

where $v \equiv |\mathbf{v}| = \sqrt{v_x^2 + v_y^2}$. Clearly, Eq. (5a) shows that the longitudinal velocity v_x is always hindered by the random force f. Equation (5b) suggests the existence of a maximum v_y at $\alpha D + f/v = G$, leading to a critical damping $\alpha_c = G/[(1 + \frac{b\Delta K^2}{Jv})D]$ that separates the boosting phase from the hindering phase. To pin a skyrmion, the random force proportional to ΔK must balance the driven force of magnitude Gu. Thus, the critical pinning disorder strength should be $\Delta K_c = cGu$ or $\Delta K_c/J = cP\mu_B/(eM_s)$, where c is a factor that depends on the skyrmion size and structure.

As shown in Fig. 7 in the plane of $\Delta K_c/J$-(αD), $\Delta K_c/J = cP\mu_B/(eM_s)$ (black line with an optimal c) separates the pinning phase from the unpinned phase, and $\alpha_c = G/[(1 + \frac{b\Delta K^2}{Jv})D]$ (red line) further separates the boosting phase from the hindering phase. Since the boundaries are obtained from

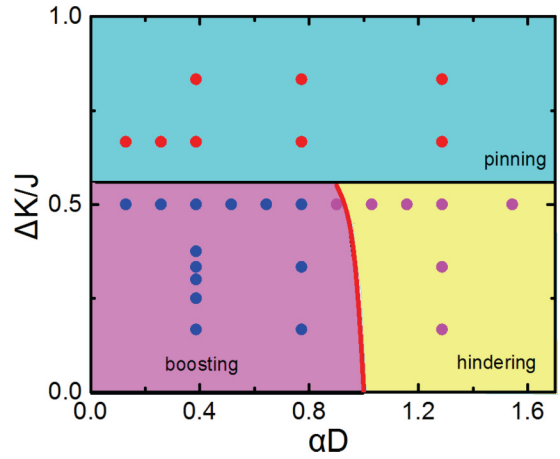

FIG. 7. Three phases in the $\Delta K/J$-αD plane. Dots are simulation results for pinning (red), boosting (blue), and hindering (purple) phases. The two boundary lines separate three phases. The black line is the pinning-unpinning boundary, while the red line is the boosting-hindering boundary

the average random force, which is smaller than the maximal possible force in the granular film, one should expect the critical disorder strength to underestimate the pinning since the maximal possible force from the random potential landscape is relevant for the pinning. Indeed, as one can see in the true simulation results (insets in Fig. 2), pinning occurs at a disorder strength below the theoretical prediction.

From Eq. (5), one can also obtain the skyrmion Hall angle

$$\theta_{\rm SH} = \tan^{-1}\left(\alpha D + \frac{\delta}{u^2}\alpha D\sqrt{1 + \alpha^2D^2}\right). \tag{6}$$

It predicts that the Hall angle decreases gradually with current density and approaches a constant value αD that is the Hall angle for the homogeneous film. As shown in Fig. 8(a), this formula (red line) could capture well the trend of the numerical results (dots). The discrepancy may come from the current density dependence of the pinning strength δ and the deformation of the moving skyrmion that are not included in our model.

IV. DISCUSSION AND CONCLUSIONS

It was known that disorders can also boost magnetic domain wall propagation [55,56]. The boosting there is related to the generation of antivortices that can both help domain wall depinning [55,56] and exert an extra driving force through the Magnus effect. Thus, it is very different from the physics of disorder-boosted transverse skyrmion motion reported here. So far, all simulations are for $\beta = 0$. In a realistic system, the fieldlike torque β should not be zero in general, although its value is believed to be small. Thus, it is natural to ask whether the physics will be different when nonzero β is considered. To address this issue, we have also carried out the same simulation for nonzero β, and the results are shown in Fig. 9. The longitudinal velocity is always hindered by the disorders, regardless of the value of β. Note that the transverse velocity reverses its sign at $\beta = \alpha$. Thus, the transverse skyrmion motion is always boosted for $\beta < \alpha$, while the boosting is

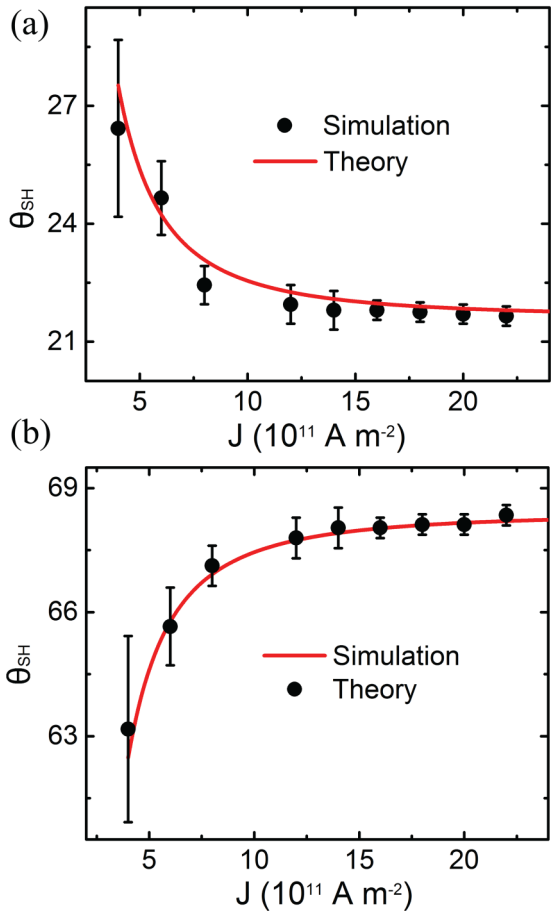

FIG. 8. The current density dependence of the skyrmion Hall angle θ_{SH} for (a) the spin-transfer-torque-driven and (b) the spin-orbit-torque-driven cases. The red lines are Eqs. (6) and (8); the black circles are numerical results. Other parameters are $\Delta K = 3\%K_0$, $\beta = 0$

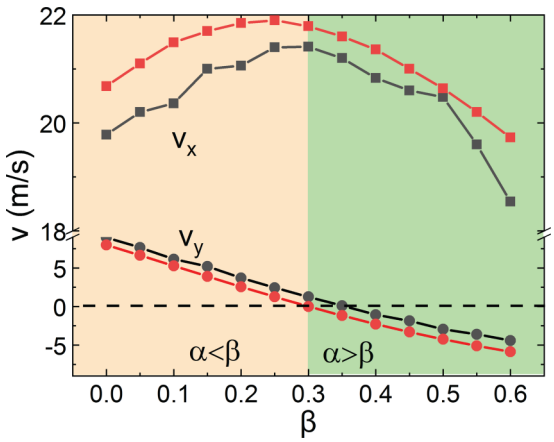

FIG. 9. The β dependence of longitudinal (squares) and transverse (dots) velocities for $\alpha = 0.3$, $J = 6 \times 10^{11}$ A/m^2 and $\Delta K = 3\%K_0$. Red denotes the velocities in the homogeneous film, while black is for the granular film.

absent when $\beta > \alpha$. Thus, the main results reported here are valid only when $\beta < \alpha$.

Surprisingly, to the best of our knowledge, no real experiments on spin-transfer-torque- (STT) driven Néel skyrmion motion have been performed, although there are many theoretical and numerical studies of STT-driven Néel skyrmion motion. A Néel skyrmion is stabilized by the interfacial DMI in experiments that is often generated at heavy-metal/ferromagnet interfaces. Naturally, such experimental systems are described by the spin-orbit-torque- (SOT) driven skyrmion motion. Thus, it should be of great interest to carry out a true experiment for STT-driven skyrmion motion. There are many ways to realize STT-driven Néel skyrmion motion. (1) One could use insulating substrates to break the inversion symmetry of the system and to generate interfacial DMI. For an insulating substrate [58], the electric current flows in the ferromagnetic layer and drives the skyrmion motion through STT. (2) The STT can come from the magnonic spin current [59] in addition to the electronic spin current. A magnonic spin current can mainly flow in the ferromagnet, and its accompanying STT can drive a Néel skyrmion to move. (3) One can also use a metallic substrate whose conductivity is much poorer than the ferromagnetic metal such that an electric current can mainly flow in the ferromagnet and drive the skyrmion by a STT.

Although our simulations and theory focus on the current-driven skyrmion motion through a STT, the physics is still valid for skyrmion motion through a spin-orbital torque, and the corresponding Thiele equation is [32,60],

$$\vec{G} \times \vec{v} + \alpha \overleftrightarrow{D} \cdot \vec{v} - \overleftrightarrow{B} \cdot \vec{u}' - \vec{F} = 0, \tag{7}$$

where the element of $\overleftrightarrow{B}$ is $B_{ij} = \iint \int (\partial_i m_z m_j - m_z \partial_i m_j) dxdy$ and $u' = (\gamma \hbar \theta_{SH})/(2eM_s d)$. The Hall angle from the new Thiele equation becomes

$$\theta_{SH} = \pi/2 - \tan^{-1}\left(\alpha D + \frac{\delta}{u^2}\alpha D\sqrt{1+\alpha^2 D^2}\right). \tag{8}$$

The current dependence of the skyrmion Hall angle has been observed in both experiments and micromagnetic simulations [32,34,38].

Figure 8(b) is a comparison of our theory with the micromagnetic simulations (dots). Different from the STT-driven case, the Hall angle increases gradually to the value of the homogeneous film with the increase of current density J. Our theory (the red line) captures well this trend.

How to manipulate and control the skyrmion Hall angle is an important issue in device applications because a nonzero Hall angle tends to push skyrmions to sample edges, leading to skyrmion annihilation. Even though the Hall effect itself comes from the skyrmion topological structure that seems to have nothing to do with disorders, two independent experiments showed recently that the skyrmion Hall angle $\theta_{SH} \equiv \arctan(v_y/v_x)$ first increases with current density and then saturates at a sufficiently large value [32,34]. So far, a good understanding of the observed behavior of the spin Hall angle is still lacking, although there are simulations [38,46] showing the saturation behavior. Most theoretical studies considered only isolated defects. Although isolated defects are important in real systems, systems with continuous random grain

boundaries may be more relevant for amorphous and polycrystal films [44,46].

It should be useful to compare our findings with recent works. Reference [39] treats skyrmions as point particles and artificially treats the disorder effect as a harmonic potential on skyrmions. This assumption is not well justified, and its prediction cannot compare to micromagnetic simulations and experiments. In contrast, our random force expression is well justified and compares with simulations. The results for the skyrmion Hall angle describe well both STT- and SOT-driven skyrmions that have opposite current dependences. Reference [47] is on the interaction of skyrmions with atomic defects in PdFe/Ir, and it is different from what we have done here. Also, the first-principles calculations are more like experiments that do not automatically provide the physics. As an example, Ref. [47] did not obtain the random force reported here. Moreover, the dynamics of skyrmions as well as the skyrmion Hall effect were not studied in the mentioned paper.

Furthermore, the pinning force expression (4) in Ref. [37] is an assumption that was initially proposed in Ref. [61] [Eq. (7)] without any true justification. There are several differences between our theory and those early works on the pinning force. First, Refs. [37,61] did not provide an explicit formula for the pinning force. In contrast, we found that the magnitude of the kinetic pinning force is given by $f = b\alpha D\Delta K^2/J$, as explained above. One can make a quantitative comparison between a theory and the simulations only when an explicit expression of the force is given. Thus, it would be very hard for Refs. [37,61] to test their theory with simulations, if not impossible. Second, the functional form of Eq. (7) in Ref. [61] is different from our pinning force. One difference is the pinning force direction when the driven current goes to zero. References [37,61] suggest it is antiparallel to the velocity, but we show it is static and transverse to the driven current. Third, the pinning force assumed in the early work has not been tested against simulations, not like what we did in the current paper. This may explain why Ref. [37] concludes a tiny disorder effect on the driven current density that is on the order of 10^5–10^6 A/m^2, inconsistent with the experimental values around 10^{10}–10^{11} A/m^2. This fact puts those disorder models as well as their theories in doubt. In our simulations, we model the disorder effect as a granular film and find that the typical driven current of a skyrmion agrees with the experimental values. Thus, we rigorously justify the kinetic pinning force.

In conclusion, we have investigated the skyrmion motion in granular magnetic films. Three phases are identified: One is the pinning phase when the disorder strength is above a critical value that depends on the driving current density. Below the critical disorder strength, the skyrmion transverse motion is boosted by the disorder below a critical damping, while the transverse motion is hindered above the critical damping. The critical damping depends also on the current density and the disorder strength. We showed that the boosting of the transverse motion is mainly due to the random force opposite the current direction. We further demonstrated that the generalized Thiele equation can perfectly capture skyrmion dynamics with a random force. Similar to the friction force in Newtonian mechanics in which static and kinetic friction forces exist, the random force on a skyrmion can be classified as the static random force and kinetic random force. For a pinned skyrmion, the static force is always against the tendency direction of skyrmion motion that is transverse to the current direction for STT-driven skyrmion motion such that the random force balances the current driving force $\vec{G} \times \vec{u}$, where $\vec{u}$ is the usual quantity that characterizes the Slonczewski spin-transfer torque. When the skyrmion is in motion, the direction of the kinetic random force is opposite the skyrmion velocity, and the value of the kinetic random force is proportional to $(\Delta K)^2/u$.

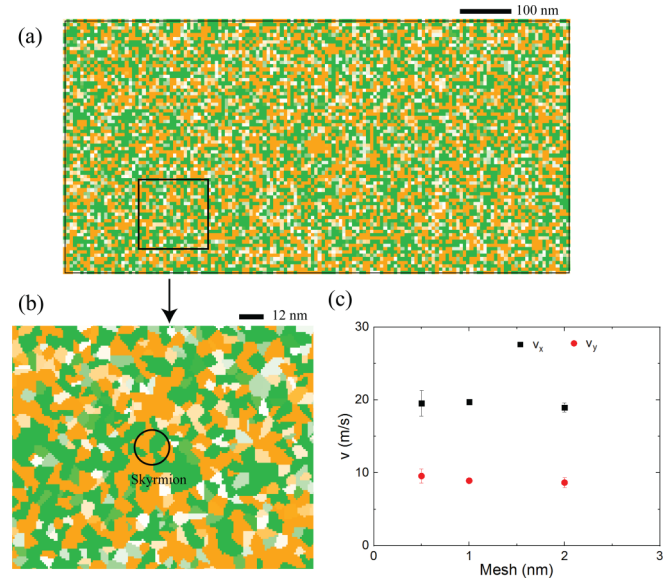

FIG. 10. (a) A typical Voronoi diagram of a magnetic film. (b) Enlarged view of the rectangle region in (a). The circle marks the size of a skyrmion. (c) The mesh size dependence of skyrmion velocities for $J = 6 \times 10^{11}$ A/m^2 and $\Delta K = 3\%K_0$, $\alpha = 0.3$.

ACKNOWLEDGMENTS

This work is supported by the National Natural Science Foundation of China (NSFC) (Grants No. 11974296 and No. 11774296) and Hong Kong RGC (Grants No. 16301518, No. 16301619, and No. 16300117). H.Y.Y. was financially supported by the NSFC (Grant No. 61704071) and the Shenzhen Fundamental Subject Research Program (Grant No. JCYJ20180302174248595).

APPENDIX

In this Appendix, we show the typical Voronoi diagram of a magnetic film in Fig. 10(a), and the typical grain size is comparable with the skyrmion size, as shown in Fig. 10(b). Furthermore, we show that reducing the mesh size below 1 nm does not change the simulation results within the model parameters used. We simulate the skyrmion velocity using different mesh sizes, as shown in Fig. 10(c). When the mesh is larger than 4 nm, the skyrmion is unstable. As the mesh decreases from 2 to 0.5 nm, the skyrmion velocity does not change significantly. This indicates that the 1-nm mesh used in the main text is sufficient.

[1] A. N. Bogdanov and U. K. Rößler, Phys. Rev. Lett. **87**, 037203 (2001).

[2] U. K. Rößler, A. N. Bogdanov, and C. Pfleiderer, Nature (London) **442**, 797 (2006).

[3] S. Mühlbauer, B. Binz, F. Jonietz, C. Pfeiderer, A. Rosch, A. Neubauer, G. Georgii, and P. Böni, Science **323**, 915 (2009).

[4] N. Romming, C. Hanneken, M. Menzel, J. E. Bickel, B. Wolter, K. von Bergmann, A. Kubetzka, and R. Wiesendanger, Science **341**, 636 (2013).

[5] X. Z. Yu, Y. Onose, N. Kanazawa, J. H. Park, J. H. Han, Y. Matsui, N. Nagaosa, and Y. Tokura, Nature (London) **465**, 901 (2010).

[6] X. Z. Yu, N. Kanazawa, Y. Onose, K. Kimoto, W. Z. Zhang, S. Ishiwata, Y. Matsui, and Y. Tokura, Nat. Mater. **10**, 106 (2011).

[7] Y. Zhou and M. A. Ezawa, Nat. Commun. **5**, 4652 (2014).

[8] H. Y. Yuan and X. R. Wang, Sci. Rep. **6**, 22638 (2016).

[9] Y. Onose, Y. Okamura, S. Seki, S. Ishiwata, and Y. Tokura, Phys. Rev. Lett. **109**, 037603 (2012).

[10] H. S. Park, X. Z. Yu, S. Aizawa, T. Tanikaki, T. Akashi, Y. Takahashi, T. Matsuda, N. Kanazawa, Y. Onose, D. Shindo, A. Tonomura, and Y. Tokura, Nat. Nanotechnol. **9**, 337 (2014).

[11] H. Du, R. Che, L. Kong, X. Zhao, C. Jin, C. Wang, J. Yang, W. Ning, R. Li, C. Jin, X. Chen, J. Zang, Y. Zhang, and M. Tian, Nat. Commun. **6**, 8504 (2015).

[12] S. Heinze, K. von Bergmann, M. Menzel, J. Brede, A. Kubetzka, R. Wiesendanger, G. Bihlmayer, and S. Blügel, Nat. Phys. **7**, 713 (2011).

[13] W. Jiang, P. Upadhyaya, W. Zhang, G. Yu, M. B. Jungfleisch, F. Y. Fradin, J. E. Pearson, Y. Tserkovnyak, K. L. Wang, O. Heinonen, S. G. E. te Velthuis, and A. Hoffmann, Science **349**, 283 (2015).

[14] J. Li, A. Tan, K. W. Moon, A. Doran, M. A. Marcus, A. T. Young, E. Arenholz, S. Ma, R. F. Yang, C. Hwang, and Z. Q. Qiu, Nat. Commun. **5**, 4704 (2014).

[15] S. Krause and R. Wiesendanger, Nat. Mater. **15**, 493 (2016).

[16] N. Nagaosa and Y. Tokura, Nat. Nanotechnol. **8**, 899 (2013).

[17] A. Fert, V. Cros, and J. Sampaio, Nat. Nanotechnol. **8**, 152 (2013).

[18] P. Dürrenfeld, Y. Xu, J. Åkerman, and Y. Zhou, Phys. Rev. B **96**, 054430 (2017).

[19] L. Kong and J. Zang, Phys. Rev. Lett. **111**, 067203 (2013).

[20] S. Rohart and A. Thiaville, Phys. Rev. B **88**, 184422 (2013).

[21] M. N. Wilson, A. B. Butenko, A. N. Bogdanov, and T. L. Monchesky, Phys. Rev. B **89**, 094411 (2014).

[22] N. Romming, A. Kubetzka, C. Hanneken, K. von Bergmann, and R. Wiesendanger, Phys. Rev. Lett. **114**, 177203 (2015).

[23] M. A. Castro and S. Allende, J. Magn. Magn. Mater. **417**, 344 (2016).

[24] X. S. Wang, H. Y. Yuan, and X. R. Wang, Commun. Phys. **1**, 31 (2018).

[25] N. Vidal-Silva, A. Riveros, and J. Escrig, J. Magn. Magn. Mater. **443**, 116 (2017).

[26] A. O. Lenov, T. L. Monchesky, N. Romming, A. Kubetzka, A. N. Bogdanov, and R. Wiesendanger, New J. Phys. **18**, 065003 (2016).

[27] H.-B. Braun, Phys. Rev. B **50**, 16485 (1994).

[28] A. Siemens, Y. Zhang, J. Hagemeister, E. Y. Vedmedenko, and R. Wiesendanger, New. J. Phys. **18**, 045021 (2016).

[29] E. Simon, K. Palotás, L. Rózsa, L. Udvardi, and L. Szunyogh, Phys. Rev. B **90**, 094410 (2014).

[30] S. Jaiswal, K. Litzius, I. Lemesh, F. Büttner, S. Finizio, J. Raabe, M. Weigand, K. Lee, J. Langer, B. Ocker, G. Jakob, G. S. D. Beach, and M. Kläui, Appl. Phys. Lett. **111**, 022409 (2017).

[31] E. A. Karhu, U. K. Rößler, A. N. Bogdanov, S. Kahwaji, B. J. Kirby, H. Fritzsche, M. D. Robertson, C. F. Majkrzak, and T. L. Monchesky, Phys. Rev. B **85**, 094429 (2012).

[32] W. Jiang, X. Zhang, G. Yu, W. Zhang, X. Wang, M. B. Jungfleisch, J. E. Pearson, X. Cheng, O. Heinonen, K. L. Wang, Y. Zhou, A. Hoffmann, and S. G. E. te Velthuis, Nat. Phys. **13**, 162 (2017).

[33] H. Y. Yuan, O. Gomonay, and M. Klaui, Phys. Rev. B **96**, 134415 (2017).

[34] K. Litzius, I. Lemesh, B. Krüger, P. Bassirian, L. Caretta, K. Richter, F. Büttner, K. Sato, O. A. Tretiakov, J. Förster, R. M. Reeve, M. Weigand, I. Bykova, H. Stoll, G. Schütz, G. S. D. Beach, and M. Kläui, Nat. Phys. **13**, 170 (2017).

[35] H. Y. Yuan, X. S. Wang, M.-H. Yung, and X. R. Wang, Phys. Rev. B **99**, 014428 (2019).

[36] S. Woo, K. Litzius, B. Krüger, M.-Y. Im, L. Caretta, K. Richter, M. Mann, A. Krone, R. M. Reeve, M. Weigand, P. Agrawal, I. Lemesh, M.-A. Mawass, P. Fischer, M. Kläui, and G. S. D. Beach, Nat. Mater. **15**, 501 (2016).

[37] J. Iwasaki, M. Mochizuki, and N. Nagaosa, Nat. Commun. **4**, 1463 (2013).

[38] C. Reichhardt, D. Ray, and C. J. Olson Reichhardt, Phys. Rev. Lett. **114**, 217202 (2015).

[39] C. Reichhardt and C. J. Olson Reichhardt, New J. Phys. **18**, 095005 (2016).

[40] J. Sampaio, V. Cros, S. Rohart, A. Thiaville, and A. Fert, Nat. Nanotechnol. **8**, 839 (2013).

[41] S.-Z. Lin, C. Reichhardt, C. D. Batista, and A. Saxena, Phys. Rev. B **87**, 214419 (2013).

[42] W. Koshibae and N. Nagaosa, Sci. Rep. **8**, 6328 (2018).

[43] R. Juge, S.-G. Je, D. de Souza Chaves, S. Pizzini, L. D. Buda-Prejbeanu, L. Aballe, M. Foerster, A. Locatelli, T. O. Mentes, A. Sala, F. Maccherozzi, S. S. Dhesi, S. Auffret, E. Gautier, G. Gaudin, J. Vogel, and O. Boulle, J. Magn. Magn. Mater. **455**, 3 (2018).

[44] J.-V. Kim and M.-W. Yoo, Appl. Phys. Lett. **110**, 132404 (2018).

[45] S. Hoshino and N. Nagaosa, Phys. Rev. B **97**, 024413 (2018).

[46] S. Woo, K. M. Song, X. Zhang, Y. Zhou, M. Ezawa, X. Liu, S. Finizio, J. Raabe, N. J. Lee, S.-I. Kim, S.-Y. Park, Y. Kim, J.-Y. Kim, D. Lee, O. Lee, J. W. Choi, B.-C. Min, H. C. Koo, and J. Chang, Nat. Commun. **9**, 959 (2018).

[47] I. L. Fernandes, J. Bouaziz, S. Blügel, and S. Lounis, Nat. Commun. **9**, 4395 (2018).

[48] R. Juge, S.-G. Je, D. de Souza Chaves, L. D. Buda-Prejbeanu, J. Peña-Garcia, J. Nath, I. M. Miron, K. G. Rana, L. Aballe, M. Foerster, F. Geunuzio, T. O. Mentes, A. Locatelli, F. Maccherozzi, S. S. Dhesi, M. Belmeguenai, Y. Roussigné, S. Auffret, S. Pizzini, G. Gaudin, J. Vogel, and O. Boulle, Phys. Rev. Applied **12**, 044007 (2019).

[49] T. Nozaki, Y. Jibiki, M. Goto, E. Tamura, T. Nozaki, H. Kubota, A. Fukushima, S. Yuasa, and Y. Suzuki, Appl. Phys. Lett. **114**, 012402 (2019).

[50] S. Zhang and Z. Li, Phys. Rev. Lett. **93**, 127204 (2004).

[51] A. Thiaville, Y. Nakatani, J. Miltat, and Y. Suzuki, Europhys. Lett. **69**, 990 (2005).
[52] A. Vansteenkiste, J. Leliaert, M. Dvornik, M. Helsen, F. Garcia-Sanchez, and F. B. V. Waeyenberge, AIP Adv. **4**, 107133 (2014).
[53] A. A. Thiele, Phys. Rev. Lett. **30**, 230 (1973).
[54] H. Y. Yuan and X. R. Wang, Phys. Rev. B **89**, 054423 (2014).
[55] H. Y. Yuan and X. R. Wang, Phys. Rev. B **92**, 054419 (2015).
[56] H. Y. Yuan and X. R. Wang, Eur. Phys. J. B **88**, 214 (2015).
[57] A. Salimath, A. Abbout, A. Brataas, and A. Manchon, Phys. Rev. B **99**, 104416 (2019).
[58] A. Qaiumzadeh, I. A. Ado, R. A. Duine, M. Titov, and A. Brataas, Phys. Rev. Lett. **120**, 197202 (2018).
[59] Y. H. Shen, X. S. Wang, and X. R. Wang, Phys. Rev. B **94**, 014403 (2016).
[60] G. Q. Yu, P. Upadhyaya, X. Li, W. Li, S. K. Kim, Y. Fan, K. L. Wong, Y. Tserkovnyak, P. K. Amiri, and K. L. Wang, Nano Lett. **16**, 1981 (2016).
[61] K. Everschor, M. Garst, B. Binz, F. Jonietz, S. Mühlbauer, C. Pfleiderer, and A. Rosch, Phys. Rev. B **86**, 054432 (2012).